Synthesis and Magnetic Properties of Colloidal $MnPt_3$ Nanocrystals

Doh C. Lee, Ali Ghezelbash, Cynthia A. Stowell, and Brian A. Korgel*

Department of Chemical Engineering, Texas Materials Institute, and Center for Nano- and Molecular Science and Technology, The University of Texas at Austin, Austin, Texas 78712

Received: June 28, 2006; In Final Form: August 22, 2006

The colloidal synthesis and magnetic properties of $MnPt_3$ nanocrystals are reported. The nanocrystal size depended on the Mn reactant used, but the Mn:Pt stoichiometry was always 1:3. As synthesized, the nanocrystals are compositionally disordered with the face-centered cubic (fcc) *A*1 phase. Annealing at 580 °C changed the $MnPt_3$ crystal structure to the compositionally ordered $L1_2$ phase ($AuCu_3$ structure) with higher magnetocrystalline anisotropy. Magnetization measurements showed that the *A*1 nanocrystals are paramagnetic and the $L1_2$ $MnPt_3$ nanocrystals are superparamagnetic.

Introduction

The quest for high-density magnetic storage media has generated the need for nanometer-size magnets as small as 2 nm.[1−4] These dimensions challenge conventional lithographic patterning approaches, and efforts have been made to develop "bottom-up" nonlithographic strategies to make nanostructured magnetic materials, such as the synthesis and self-assembly of colloidal magnetic nanocrystals.[5−9] A wide variety of magnetic nanocrystals, including γ-Fe_2O_3,[10,11] Ni,[12,13] Co,[14−18] FePt,[6,9] $CoPt_3$,[19] MnPt,[20] $CoFe_2O_4$,[21,22] and $MnFe_2O_4$,[23] have been synthesized in solution by use of organometallic reactants as starting materials with organic capping ligands to control their size. In some cases, these syntheses have been scaled to large quantities (∼grams) while still maintaining tight size control.[24] The nanocrystal size, shape, composition, and reaction yields all depend on the organometallic decomposition chemistry and the particle growth kinetics.[25] This is especially true in the synthesis of nanocrystal materials with complicated phase behavior, in which subtle changes in reactant chemistry and reaction conditions can rather dramatically change the nanocrystal composition, shape, and crystal structure.[18,26,27]

Nanocrystals of M−Pt (M = transition metal, such as Fe or Co) alloys have been the focus of recent synthetic interest because their high magnetocrystalline anisotropy is needed for long-term stable magnetic memory. Colloidal syntheses have been developed to produce various M−Pt nanocrystals, such as FePt and $CoPt_3$, with very good size control, but the crystalline cores are compositionally disordered with weak magnetic properties.[6,7,9,19] The nanocrystals therefore require high-temperature annealing to convert their crystal structure to a compositionally ordered phase with large magnetocrystalline anisotropy.

Here, we demonstrate the colloidal synthesis of $MnPt_3$ nanocrystals. Mn−Pt is an interesting alloy because it exhibits composition-dependent magnetic properties that range from antiferromagnetic (MnPt) to fully ferromagnetic ($MnPt_3$).[28−30] The magnetic properties arise from exchange coupling between Mn−Mn spins, which depends on the Mn−Mn atomic separation, crystal symmetry, and lattice position. $MnPt_3$ has also been reported to have a large magnetooptic response and could be suitable for magnetooptic information storage media using blue light.[31−33] We were also particularly interested in making Mn−Pt nanocrystals because of a recent report by Ono et al.,[20] who found that Mn−Pt nanocrystals with a molar ratio of 52.5:47.5 exhibited ferromagnetism even though this composition should be antiferromagnetic. The observed ferromagnetism presumably resulted from the small size of the nanocrystals and their high surface area-to-volume ratio.[20] In our synthesis, we were only able to achieve Mn−Pt nanocrystals with 1:3 Mn:Pt stoichiometry. The nanocrystals obtained from the synthetic reaction are chemically disordered with Mn and Pt in an fcc unit cell—the *A*1 phase. By annealing films of the nanocrystals at 580 °C, the particles are converted from the *A*1 phase to the compositionally ordered $L1_2$ phase ($AuCu_3$ structure) that is ferromagnetic with a Curie temperature of 380 K in the bulk.[33] X-ray diffraction (XRD) and transmission electron microscopy (TEM) reveal that the annealed films have significant aggregation and coalescence of the primary particles, as has been observed for annealed films of organic ligand-coated FePt nanocrystals.[34]

Experimental Details

Mn−Pt nanocrystals were produced by high-temperature reduction of platinum acetylacetonate [$Pt(acac)_2$, Aldrich] with 1,2-hexadecanediol (Aldrich), in the presence of either manganese acetylacetonate [$Mn(acac)_2$, Aldrich] or dimanganese decacarbonyl [$Mn_2(CO)_{10}$, Aldrich]. All syntheses were carried out by standard airless procedures on a Schlenk line with commercially available reagents.

Synthesis Using $Mn_2(CO)_{10}$ as the Mn Source. $Pt(acac)_2$ (197 mg, 0.5 mmol) and 1,2-hexadecanediol (646 mg, 2.5 mmol) were added to 20 mL of dioctyl ether (Fluka). The mixture was stirred and purged with nitrogen at room temperature for 30 min. The solution is cloudy at this point. The solution was then heated to 100 °C, and upon heating the solution becomes optically clear. At 100 °C, a solution of 0.5 mmol $Mn_2(CO)_{10}$ in 12 mL of dioctyl ether was injected into the reaction flask, followed by additional oleic acid (Aldrich) (1.30 mL, 4 mmol) and oleylamine (Aldrich) (1.35 mL, 4 mmol). The reaction mixture was heated at a rate of 5 °C/min to reflux at 297 °C. During heating, the solution turns black at ∼170 °C, indicating

* To whom correspondence should be addressed: phone +1-512-471-5633; fax +1-512-471-7060; e-mail korgel@mail.che.utexas.edu.

10.1021/jp064050n CCC: $33.50
Published on Web 09/27/2006

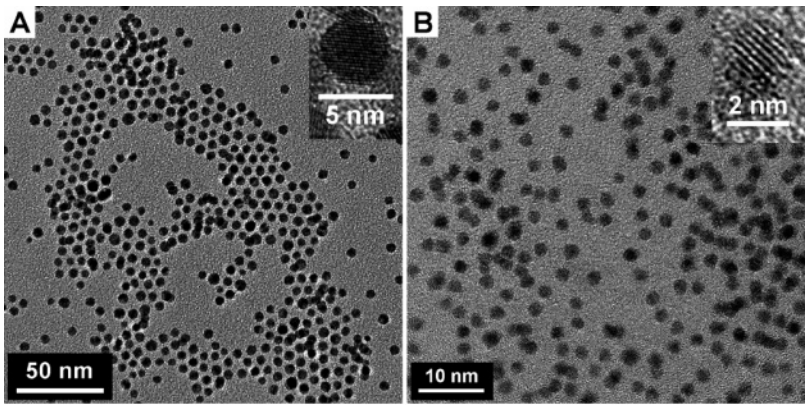

Figure 1. TEM images of $MnPt_3$ nanocrystals synthesized by reducing $Pt(acac)_2$ in the presence of (A) $Mn_2(CO)_{10}$ or (B) $Mn(acac)_2$.

the onset of particle growth. After 30 min of heating at the reflux temperature, the heating element was removed from the flask and the solution was allowed to cool to room temperature.

Synthesis Using $Mn(acac)_2$ as the Mn Source. $Pt(acac)_2$ (197 mg, 0.5 mmol) and $Mn(acac)_2$ (126 mg, 0.5 mmol) were added to a solution of 1,2-hexadecandiol (160 mg, 1 mmol) in 10 mL of dioctyl ether. The mixture was heated to 100 °C, and oleic acid (158 μL, 0.5 mmol) and oleylamine (164 μL, 0.5 mmol) were introduced to the flask. The reaction mixture was then heated to reflux at 297 °C under vigorous stirring. After 30 min of heating at the reflux temperature, the heating mantle was removed and the solution was allowed to cool to room temperature.

Purification and Annealing. The product was collected in a 50 mL centrifuge tube and then size-selected and washed by the following method: 5 mL of hexane, 100 μL of oleic acid, and 100 μL of oleylamine were added to the product solution. The solution was then centrifuged at 8000 rpm for 10 min. A precipitate formed that was brown, and energy-dispersive spectrometry (EDS) analysis showed that there was a significant population of Mn-rich particles 15−30 nm in diameter. Ethanol (60 mL) was then added to the supernatant and the mixture was centrifuged at 8000 rpm for 10 min. The precipitate was collected and stored in a hexane solution. For the annealing, concentrated hexane dispersions of nanocrystals (~10 mg/mL) were drop-cast on a Si substrate. The substrate was placed in a tube furnace (Lindberg, Blue M) and annealed at 580 °C for 30 min under nitrogen. A thermocouple was placed in close proximity to the substrate holder to ensure the accuracy of the temperature measurement. The heating rate was ~55 °C/min.

Characterization. The nanocrystals were characterized by transmission electron microscopy (TEM), X-ray diffraction (XRD), and magnetization measurements. Samples were prepared for TEM by drop-casting from chloroform onto carbon-coated Cu TEM grids (200-mesh, LADD science). TEM images were acquired at 200 kV accelerating voltage on a JEOL 2010F equipped with an energy-dispersive X-ray spectrometer (EDS, Gatan). The magnetic properties of the nanocrystals were measured using a superconducting quantum interference device (SQUID, Quantum Design, Inc.) magnetometer. The particles, either as-made or annealed, were collected by drop-casting from a chloroform dispersion onto a silicon substrate and by scraping the dried film into a gelatin capsule (Eli Lilly and Co.). The capsule was inserted into the magnetometer and centered under a field at 1 kOe at 5 K, before temperature-sweep scans were started. The temperature-sweep scan data were collected at a constant field at 1 kOe with temperatures ranging from 5 to 300 K. The magnetization was also measured as a function of applied field at 5 and 300 K. XRD was performed on a Bruker-Nonius D8 Advance θ-2θ powder diffractometer with Cu K_α radiation (λ = 1.54 Å). Samples were prepared for XRD by drop-casting a concentrated dispersion of nanocrystals onto a quartz substrate to give a film ~200 μm thick. XRD scans were acquired at 12 deg/min in 0.02 deg increments, while simultaneously rotating the sample at 15 deg/min. Diffraction patterns were collected for 10−12 h.

Results

$MnPt_3$ Nanocrystal Synthesis. Figure 1 shows Mn−Pt nanocrystals obtained from reactions with $Pt(acac)_2$ and either $Mn_2(CO)_{10}$ or $Mn(acac)_2$ as the Mn source. EDS mapping of individual particles, as well as from fields of particles, revealed that the particles have an Mn:Pt ratio of 1:3, regardless of which Mn precursor was used. The average diameter of the $MnPt_3$ nanocrystals depended on the Mn reactant used. $Mn_2(CO)_{10}$ gave larger nanocrystals, approximately 5 nm in diameter, and $Mn(acac)_2$ gave smaller nanocrystals approximately 2 nm in diameter. The size difference appears to originate from the difference in decomposition rates of the two reactants. We found that nanocrystal reactions proceeded faster with $Mn_2(CO)_{10}$ than $Mn(acac)_2$, presumably due to its higher decomposition rate.

Under all reaction conditions explored, the Mn−Pt composition of the nanocrystals was found to be $MnPt_3$. Other intermetallic phases such as MnPt were never obtained, regardless of how the Mn precursors were added to the reaction (e.g., Mn first followed by Pt). $MnPt_3$ nanocrystals were still obtained when the Mn reactant was added in excess, but with the addition of pure Mn nanocrystals larger than 10 nm in diameter. The more Mn reactant added, the more Mn particles that were formed, and we could not find any reaction conditions to incorporate additional Mn into the nanocrystals.

Figure 2 shows TEM images of nanocrystals synthesized with both $Mn_2(CO)_{10}$ and $Mn(acac)_2$ before and after size-selective precipitation. Both Mn reactants yielded large (>10 nm diameter) Mn particles when the reaction stoichiometry was greater than 1:3 Mn:Pt (i.e., excess Mn). Since the Mn particles are much larger than the $MnPt_3$ nanocrystals, size-selective precipitation easily removes these particles to give a pure $MnPt_3$ product. Figure 3 shows more TEM images of $MnPt_3$ and Mn nanocrystals obtained in reactions with $Mn_2(CO)_{10}$ with increasing Mn:Pt ratios in the reaction media. Mn:Pt ratios of 1:3 gave almost exclusively $MnPt_3$ nanocrystals (Figure 3A). Increasing the $Mn_2(CO)_{10}$ concentration increased the relative amount of Mn particles.

To understand the role of the Mn reactant on nanocrystal synthesis, reactions were carried out in the absence of $Pt(acac)_2$ with only $Mn_2(CO)_{10}$. It turns out that the reducing agent, 1,2-

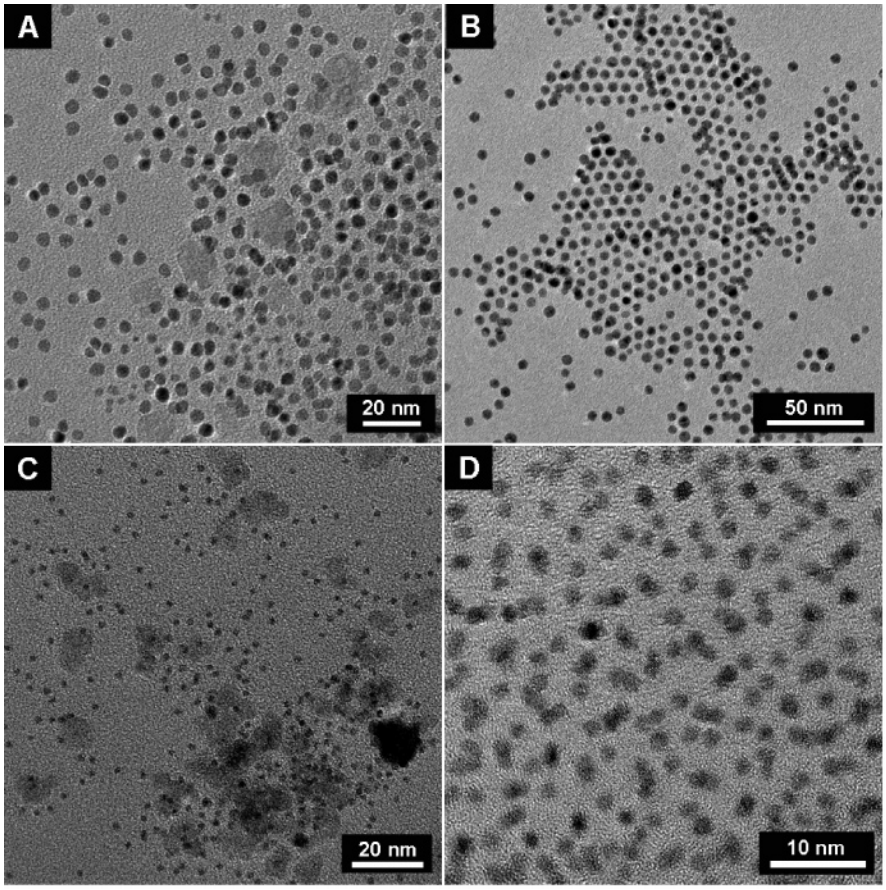

Figure 2. TEM images of the nanocrystal product before (A, C) and after (B, D) size-selective precipitation from reactions with (A, B) $Mn_2(CO)_{10}$ and (C, D) $Mn(acac)_2$ as the Mn source. In panels A and C, the large faint particles are pure Mn particles and the smaller darker particles are $MnPt_3$. The Mn particles are larger than 10 nm in diameter and are removed from the sample by size-selective precipitation, as confirmed by their absence in panels B and D.

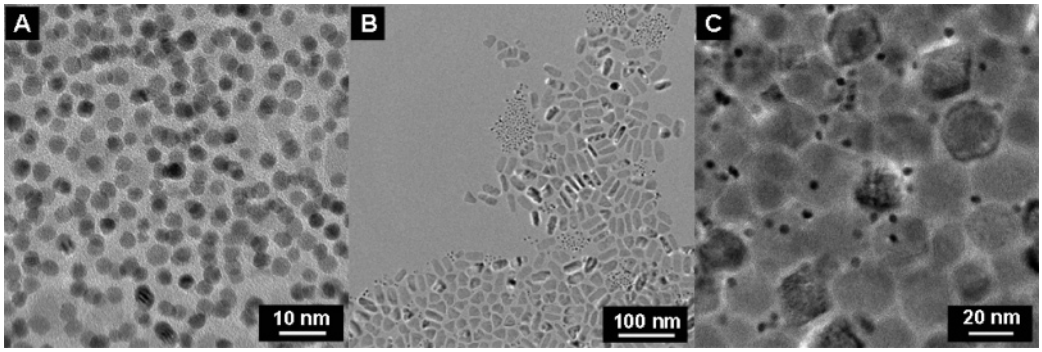

Figure 3. TEM images of nanocrystals synthesized with different Mn:Pt precursor ratios with $Mn_2(CO)_{10}$ as the Mn source. The Mn:Pt reactant mole ratios were varied from (A) 0.7:1, (B) 3:1, and (C) 3:1 with phenyl ether used as the solvent instead of dioctyl ether. (A) There are very few Mn particles—the small dark particles in the TEM are $MnPt_3$. (B) The rod-shaped and triangular particles are pure Mn and the very small (5 nm diameter) dark particles are $MnPt_3$. (C) The large rectangular nanocrystals ~20 nm in diameter are crystalline Mn particles and the small (<5 nm diameter) dark particles are $MnPt_3$.

hexadecanediol, strongly influences the Mn nanocrystal size and shape as shown in Figure 4. With 1,2-hexadecanediol added to the reaction, Mn nanocrystals form with irregular shape. Without the diol, the Mn nanocrystals are spherical with relatively narrow size distributions.

$MnPt_3$ Structural and Magnetic Phase Behavior upon Annealing. Figure 5 shows XRD data obtained from $MnPt_3$ nanocrystals after all the Mn particulate byproducts were removed by size-selective precipitation. The $MnPt_3$ nanocrystals exhibit the *A*1 phase of $MnPt_3$ that has a compositionally disordered face-centered cubic (fcc) unit cell (JCPDS number 65-5033). When the nanocrystals are annealed at 580 °C and above, new diffraction peaks appeared as shown in Figure 5, which can be assigned to the (100), (110), (210), (211), (221), and (310) lattice planes of $L1_2$ $MnPt_3$ (JCPDS number 65-3260). $L1_2$ $MnPt_3$ has atomically ordered Mn and Pt atoms in the unit cell: Mn occupies the corner positions of the unit cell and the Pt occupies the face centers. No significant structural change was detected when the nanocrystals were annealed at temperatures below 500 °C.

After annealing of the nanocrystals at 580 °C, the XRD peaks have also noticeably sharpened, indicating that there sintering and grain growth of the particles occurs in the nanocrystal film. The average $MnPt_3$ crystalline grain sizes determined by use of the Scherrer equation were 4.3 and 7.0 nm before and after annealing [with $Mn_2(CO)_{10}$] and 1.7 and 5.8 nm before and after

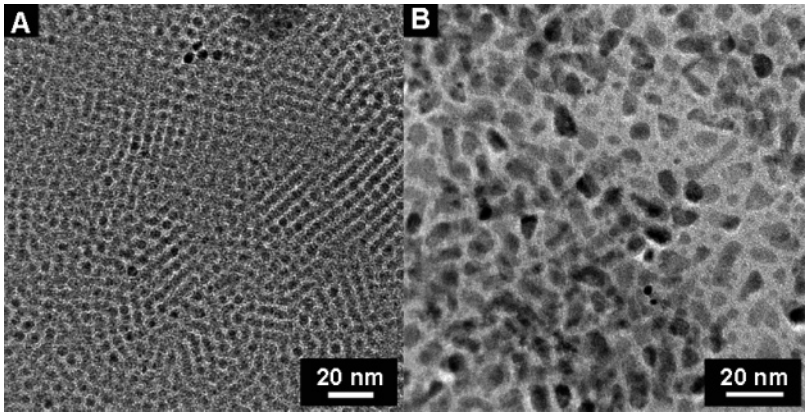

Figure 4. Mn nanocrystals synthesized by reacting $Mn_2(CO)_{10}$ in dioctyl ether at 300 °C for 30 min (A) without and (B) with 1,2-hexadecanediol. Without diol addition, spherical Mn nanocrystals form with a narrow size distribution. The diol stimulates the formation of large irregular-shaped Mn nanocrystals.

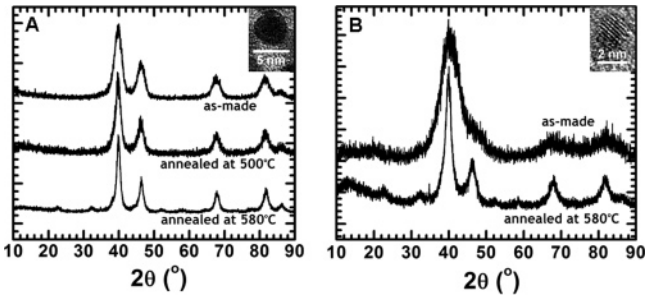

Figure 5. XRD of $MnPt_3$ nanocrystals synthesized with (a) $Mn_2(CO)_{10}$ and (b) $Mn(acac)_2$ as the Mn reactant. By use of the Scherrer equation to determine the average particle diamater, the nanocrystals have average diameters of (a) 4.3 and (b) 1.7 nm. The XRD patterns of as-made nanocrystals match with the fcc *A*1 structure (JCPDS 65-5033). The patterns of annealed sample index to the $L1_2$ phase of $MnPt_3$ (JCPDS 65-3260).

annealing [with $Mn(acac)_2$]. The smaller 1.7 nm diameter nanocrystals made with $Mn(acac)_2$ undergo a proportionally larger size increase and more dramatic peak sharpening in the XRD pattern, although the final particle diameters are similar for both samples: 7.0 versus 5.8 nm. Sintering of organic ligand-coated nanocrystals annealed at temperatures above ~500 °C is well-known.[7,34,35]

Figure 6 shows temperature-dependent zero-field-cooled (ZFC) and field-cooled (FC) magnetization scans under an applied field of 1000 Oe for 4.3 nm diameter $MnPt_3$ nanocrystals synthesized with $Mn_2(CO)_{10}$ before and after annealing at 580 °C. Before annealing, the nanocrystals are paramagnetic. After annealing at 580 °C, the nanocrystals become superparamagnetic with a blocking temperature at approximately 30 K. The Curie temperature of bulk $L1_2$ $MnPt_3$ is 380 K.[33] The field sweep of the annealed particles at 5 K exhibits hysteresis with a coercivity of ~500 Oe (Figure 6D). The change in magnetic properties results from the phase change from paramagnetic *A*1 $MnPt_3$ to ferromagnetic $L1_2$ $MnPt_3$ upon annealing.

Figure 7 shows temperature-dependent zero-field-cooled (ZFC) magnetization scans under an applied field of 1000 Oe for 1.7 nm diameter $MnPt_3$ nanocrystals synthesized with $Mn(acac)_2$ before and after annealing at 580 °C. The magnetic properties of these $MnPt_3$ nanocrystals were qualitatively similar to those of the nanocrystals synthesized with $Mn_2(CO)_{10}$ as the Mn source measured in Figure 6: the as-synthesized *A*1 $MnPt_3$ nanocrystals were paramagnetic and the annealed $MnPt_3$ nanocrystals were superparamagnetic. However, the blocking temperature of the annealed nanocrystals made with $Mn(acac)_2$ was significantly higher than the annealed particles made with $Mn_2(CO)_{10}$ at ~100 K (Figure 7B). The coercivity at 5 K was also significantly higher: 2.2 kOe versus only 500 Oe. Larger particle size should give higher blocking temperatures of superparamagnetic particles. However, this is not the case here, as the average particle diameter determined from the peak breadth in XRD was 5.8 nm, which is smaller than the nanocrystals made with $Mn_2(CO)_{10}$ after annealing (7.0 nm). The magnetic properties of $MnPt_3$ are also very sensitive to Mn−Pt composition and atomic order. Although the analysis of the particles by EDS and XRD did not reveal a noticeable difference in Mn:Pt ratio, if the $MnPt_3$ nanocrystals synthesized with $Mn_2(CO)_{10}$ were slightly Mn-poor there would be weaker ferromagnetic coupling between Mn spins, which leads to a decreased coercivity and Curie temperature in bulk $MnPt_3$ and would lead to a decreased blocking temperature in the nanocrystals.[32]

Coupled $MnPt_3$ Nanocrystals. Figure 8 shows a TEM image of a sample obtained from the reaction with $Mn_2(CO)_{10}$ as a Mn source. Although most of the TEM grid was covered with nanocrystals separated by at least a few nanometers, some of the $MnPt_3$ particles form pairs with a shared crystallographic orientation with their ⟨111⟩ direction of the $MnPt_3$ unit cell perpendicular to their shared interface. It is unclear what the pairing mechanism is; however, perhaps the different Pt atom population on {111} facets leads to oriented attachment.[36,37]

Discussion

To probe more effectively the influence of particle size and composition on the magnetic properties of the $L1_2$ $MnPt_3$ nanocrystals, it would be desirable to encapsulate them in a ceramic coating that can withstand the annealing temperatures and prevent sintering. We recently reported the encapsulation of FePt nanocrystals in SiO_2 that was able to prevent sintering during high-temperature annealing.[7] We tried this coating chemistry on the $MnPt_3$ nanocrystals; however, the particles chemically degraded during the coating procedure. The Mn appears to be more sensitive to oxidation than Fe, and the strong base required for SiO_2 formation appears to attack Mn in the particles. New coating chemistry that is less aggressive is needed for this system.

It is also worth noting that the chemical approach to $MnPt_3$ nanocrystals developed here is very similar to the chemistry used by Ono et al.[20] to make MnPt nanocrystals. We were unable to find conditions suitable to make MnPt, and excess Mn reactant only generated pure Mn particles in the presence of $MnPt_3$ nanocrystals. It is possible that the MnPt nanocrystals reported by Ono et al.[20] were in fact $MnPt_3$ contaminated with

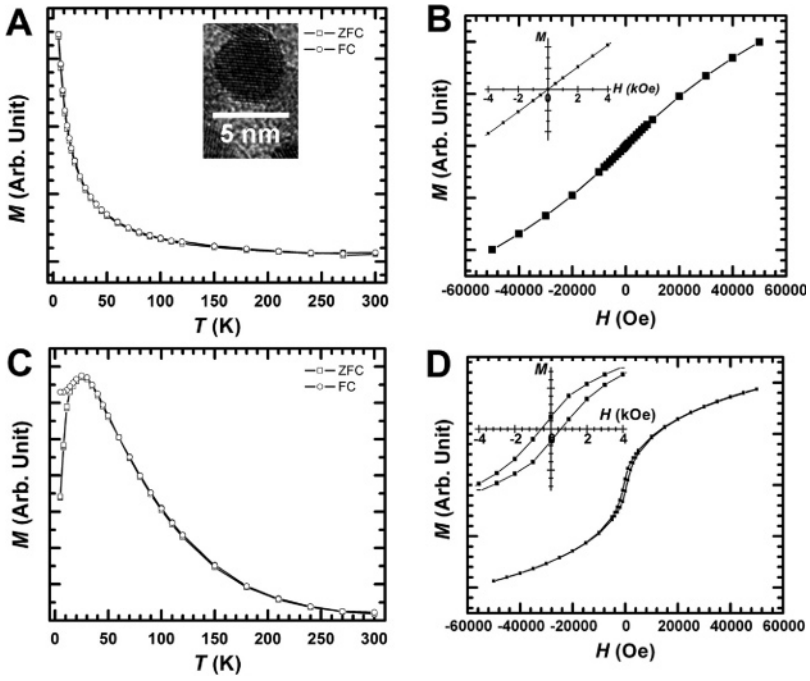

Figure 6. Magnetization measurements of 4.3 nm diameter $MnPt_3$ nanocrystals synthesized with $Mn_2(CO)_{10}$ (A, B) before and (C, D) after annealing at 580 °C: (A, C) field-cooled and zero-field-cooled scans and (B, D) field sweeps at 5 K. No hysteresis is seen in panel B), while the plot in panel D shows the coercivity of ~500 Oe. [Insets in panels B and D are magnifications of the field sweeps near zero field to magnify the hysteresis]. Note that sintering occurred during annealing and increased the average particle diameter to 7.0 nm, as determined by the Scherrer equation from XRD.

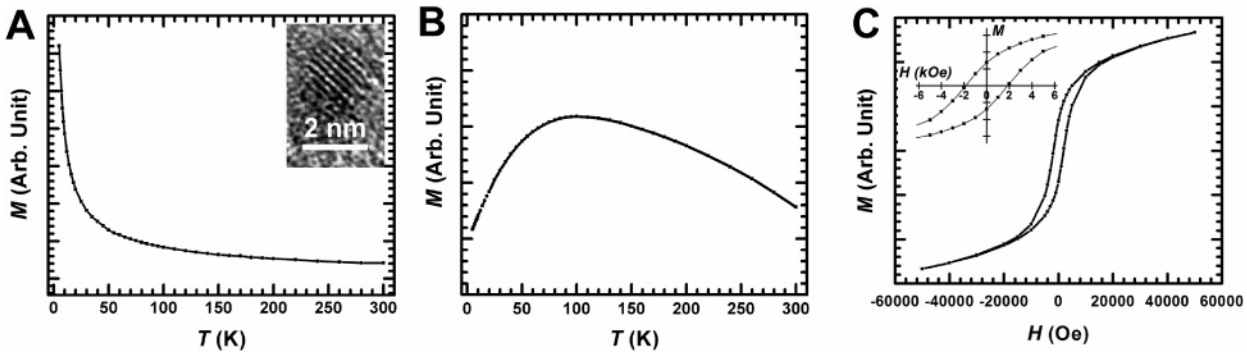

Figure 7. Magnetic properties of 1.7 nm diameter $MnPt_3$ nanocrystals synthesized with $Mn(acac)_2$: zero-field-cooled (ZFC) temperature-dependent magnetization scans under an applied field of 1000 Oe (A) before and (B) after annealing at 580 °C. Annealing at 580 °C led to sintering and an increase in average particle diameter of 5.8 nm determined from the Scherrer equation and the peak breadth in the XRD patterns. (C) Field sweep of the magnetization of the annealed nanocrystals at 5 K; the coercivity is 2.2 kOe.

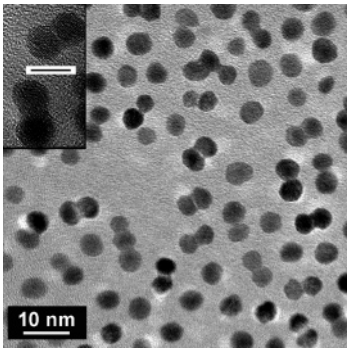

Figure 8. TEM image of $MnPt_3$ nanocrystals synthesized with $Pt(acac)_2$ and $Mn_2(CO)_{10}$. The TEM sample was prepared by drop-casting a hexane dispersion of $MnPt_3$ nanocrystals. Several nanocrystals are paired along the ⟨111⟩ direction of the $MnPt_3$ unit cell. The scale bar in the inset is 5 nm.

Mn nanocrystals, which would explain their observation of ferromagnetic spin coupling in their system. Furthermore, they did not see a phase transition from cubic to tetragonal crystal structure in XRD of their materials after annealing, as would be expected from $L1_0$ MnPt, which has a tetragonal unit cell. Certainly more study of Mn−Pt nanocrystals is needed to fully clarify the properties of these materials and the relationship between synthetic conditions and the composition, crystal structure, and their magnetic properties.

Conclusions

$MnPt_3$ nanocrystals were synthesized by a colloidal approach. It was not possible to influence the Mn:Pt stoichiometry in our synthesis, and at higher Mn concentrations, pure Mn particles were produced in addition to $MnPt_3$ nanocrystals. The $MnPt_3$ nanocrystals obtained from the reaction have the chemically disordered fcc *A*1 phase. Annealing films of the nanocrystals at 580 °C converted the nanocrystals to the compositionally ordered $L1_2$ phase ($AuCu_3$ structure). These annealed films were superparamagnetic.

Acknowledgment. This research was supported by funding from the National Science Foundation (NIRT program DMR-0210383; STC program CHE-9876674), the Robert A. Welch Foundation, and the Advanced Prototype and Processing Center (AP2C, DARPA HR00011-06-1-0005).

References and Notes

(1) Murdock, E. S.; Simmons, R. F.; Davidson, R. *IEEE Trans. Magn.* **1992**, *28*, 3078.

(2) Grochowski, E.; Thompson, D. A. *IEEE Trans. Magn.* **1994**, *30*, 3797.

(3) Lambeth, D. N.; Velu, E. M. T.; Bellesis, G. H.; Lee, L. L.; Laughlin, D. E. *J. Appl. Phys.* **1996**, *79*, 4496.

(4) Moser, A.; Takano, K.; Margulies, D. T.; Albrecht, M.; Sonobe, Y.; Ikeda, Y.; Sun, S. H.; Fullerton, E. E. *J. Phys. D: Appl. Phys.* **2002**, *35*, R157.

(5) Hyeon, T. *Chem. Commun.* **2003**, 927.

(6) Sun, S. H.; Murray, C. B.; Weller, D.; Folks, L.; Moser, A. *Science* **2000**, *287*, 1989.

(7) Lee, D. C.; Mikulec, F. V.; Pelaez, J. M.; Koo, B.; Korgel, B. A. *J. Phys. Chem. B* **2006**, *110*, 11160.

(8) Zeng, H.; Li, J.; Liu, J. P.; Wang, Z. L.; Sun, S. H. *Nature* **2002**, *420*, 395.

(9) Sun, S. H. *Adv. Mater.* **2006**, *18*, 393.

(10) Park, S. J.; Kim, S.; Lee, S.; Khim, Z. G.; Char, K.; Hyeon, T. *J Am. Chem. Soc.* **2000**, *122*, 8581.

(11) Hyeon, T.; Lee, S. S.; Park, J.; Chung, Y.; Bin Na, H. *J. Am. Chem. Soc.* **2001**, *123*, 12798.

(12) Cordente, N.; Respaud, M.; Senocq, F.; Casanove, M. J.; Amiens, C.; Chaudret, B. *Nano Lett.* **2001**, *1*, 565.

(13) Murray, C. B.; Sun, S.; Doyle, H.; Betley, T. *MRS Bull.* **2001**, *26*, 985.

(14) Sun, S. H.; Murray, C. B. *J. Appl. Phys.* **1999**, *85*, 4325.

(15) Puntes, V. F.; Zanchet, D.; Erdonmez, C. K.; Alivisatos, A. P. *J. Am. Chem. Soc.* **2002**, *124*, 12874.

(16) Dinega, D. P.; Bawendi, M. G. *Angew. Chem., Int. Ed.* **1999**, *38*, 1788.

(17) Dumestre, F.; Chaudret, B.; Amiens, C.; Fromen, M. C.; Casanove, M. J.; Renaud, P.; Zurcher, P. *Angew. Chem., Int. Ed.* **2002**, *41*, 4286.

(18) Puntes, V. F.; Krishnan, K. M.; Alivisatos, A. P. *Science* **2001**, *291*, 2115.

(19) Shevchenko, E. V.; Talapin, D. V.; Schnablegger, H.; Kornowski, A.; Festin, O.; Svedlindh, P.; Haase, M.; Weller, H. *J. Am. Chem. Soc.* **2003**, *125*, 9090.

(20) Ono, K.; Okuda, R.; Ishii, Y.; Kamimura, S.; Oshima, M. *J. Phys. Chem. B* **2003**, *107*, 1941.

(21) Hyeon, T.; Chung, Y.; Park, J.; Lee, S. S.; Kim, Y. W.; Park, B. H. *J. Phys. Chem. B* **2002**, *106*, 6831.

(22) Song, O.; Zhang, Z. J. *J. Am. Chem. Soc.* **2004**, *126*, 6164.

(23) Kang, E.; Park, J.; Hwang, Y.; Kang, M.; Park, J. G.; Hyeon, T. *J. Phys. Chem. B* **2004**, *108*, 13932.

(24) Park, J.; An, K. J.; Hwang, Y. S.; Park, J. G.; Noh, H. J.; Kim, J. Y.; Park, J. H.; Hwang, N. M.; Hyeon, T. *Nat. Mater.* **2004**, *3*, 891.

(25) Park, J.; Lee, E.; Hwang, N. M.; Kang, M. S.; Kim, S. C.; Hwang, Y.; Park, J. G.; Noh, H. J.; Kini, J. Y.; Park, J. H.; Hyeon, T. *Angew. Chem., Int. Ed.* **2005**, *44*, 2872.

(26) Stowell, C. A.; Wiacek, R. J.; Saunders, A. E.; Korgel, B. A. *Nano Lett.* **2003**, *3*, 1441.

(27) Ghezelbash, A.; Korgel, B. A. *Langmuir* **2005**, *21*, 9451−9456.

(28) Kim, W.; Hong, S. C.; Seo, J.; Oh, S.-J.; Min, H. G.; Kim, J.-S. *Phys. Rev. B* **2004**, *70*, 174453.

(29) Pickart, S. J.; Nathans, R. *J. Appl. Phys.* **1962**, *33*, 1336.

(30) Kren, E.; Kadar, G.; Pal, L.; Solyom, J.; Szabo, P.; Tarnoczi, T. *Phys. Rev.* **1968**, *171*, 574.

(31) Kato, T.; Kikusawa, H.; Iwata, S. W.; Tsuanashima, S.; Uchiyama, S. *J. Magn. Magn. Mater.* **1995**, *140*, 713.

(32) Wierman, K. W.; Kirby, R. D. *J. Magn. Magn. Mater.* **1996**, *154*, 12.

(33) Wierman, K. W.; Hilfiker, J. N.; Sabiryanov, R. F.; Jaswal, S. S.; Kirby, R. D.; Woollam, J. A. *Phys. Rev. B* **1997**, *55*, 3093.

(34) Ding, Y.; Majetich, S. A.; Kim, J.; Barmak, K.; Rollins, H.; Sides, P. *J. Magn. Magn. Mater.* **2004**, *284*, 336.

(35) Hyun, C.; Lee, D. C.; Israel, C.; Korgel, B. A.; de Lozanne, A. *IEEE Trans. Magn.* **2006** (submitted for publication).

(36) Cho, K. S.; Talapin, D. V.; Gaschler, W.; Murray, C. B. *J. Am. Chem. Soc.* **2005**, *127*, 7140.

(37) Penn, R. L. *J. Phys. Chem. B* **2004**, *108*, 12707.